Clim Dyn
DOI 10.1007/s00382-016-3181-9

Unusual growth in intense typhoon occurrences over the Philippine Sea in September after the mid-2000s

Haozhe He[1,2] · Jing Yang[1,2] · Liguang Wu[3] · Daoyi Gong[1,2] · Bin Wang[4,5] · Miaoni Gao[1,2]

Received: 13 October 2015 / Accepted: 18 May 2016

Abstract During the global warming hiatus period (1998–present), a pronounced increase in the number of intense typhoon occurrences was identified over the Philippine Sea (PS: 5°–25°N, 125°–140°E) in September after the mid-2000s. Comparing two periods before and after the mid-2000s indicates that intense typhoons rarely occurred over the PS in September before the mid-2000s, with a frequency of fewer than 0.4 per year, but reached up to nearly 1.5 per year after the mid-2000s. The abrupt increase in intense typhoon occurrences over the PS was primarily attributed to increased tropical cyclone (TC) genesis and favorable large-scale conditions for TC intensification. The increase in TC genesis number over the PS was caused by contributory dynamical conditions, including positive low-level relative vorticity anomalies and anomalous ascents, which corresponded to a southwestward shift and strengthening of the monsoon trough. In addition, among the favorable large-scale conditions, the increased relative humidity that resulted from intensified moisture flux convergence exerted essential effect on the TC intensification. These changes in atmospheric environmental conditions favoring intense typhoon occurrences over the PS were primarily associated with the change in the tropical Indo-Pacific sea surface temperature (SST) around the mid-2000s. Besides that, the positive feedback TCs exerted on the circulation was also conducive to the unusual growth in intense typhoon occurrences over the PS. And note that the role of SST anomalies in the air–sea interaction is the key to interpret why the unique phenomenon only occurred in September.

Keywords Intense typhoon · The Philippine Sea · Unusual growth · Tropical Indo-Pacific sea surface temperature

✉ Jing Yang
yangjing@bnu.edu.cn

[1] State Key Laboratory of Earth Surface Processes and Resource Ecology (ESPRE), Beijing Normal University, Beijing 100875, China

[2] Academy of Disaster Reduction and Emergency Management, Ministry of Civil Affairs and Ministry of Education, Beijing Normal University, Beijing 100875, China

[3] Key Laboratory of Meteorological Disaster of Ministry of Education, and Pacific Typhoon Research Center, Nanjing University of Information Science and Technology, Nanjing 210044, China

[4] Department of Atmospheric Sciences, and International Pacific Research Center, University of Hawaii at Manoa, Honolulu, Hawaii 96825, USA

[5] Earth System Modeling Center, Nanjing University of Information Science and Technology, Nanjing 210044, China

1 Introduction

Tropical cyclones (TCs) account for a significant fraction of damage, injury and loss of life from natural hazards and are the costliest natural catastrophes in coastal areas (Zhang et al. 2009; Peduzzi et al. 2012). As the most prolific generator of TCs, the western North Pacific (WNP) suffers from approximately one-third of the total global TC occurrences (Chan 2005). Hence, characterizing and understanding the long-term changes of WNP TC activity, which is crucial for regional TC forecasts and disaster reduction, has become an essential research subject, particularly in East Asia. Recently, a number of studies have reported that WNP TC activity (e.g., genesis, occurrence frequency and tracks) experienced significant decadal variability in the late 1990s,

Published online: 28 May 2016

which has been well known in the scientific community to be a climate regime shift point (e.g., McPhaden et al. 2011; Hong et al. 2014). The decadal change in WNP TC activity is mostly attributed to atmospheric dynamical contributors (i.e., low-level relative vorticity, vertical velocity, vertical wind shear), which are the response to the change in the tropical Indo-Pacific sea surface temperature (SST) in the late 1990s (Tu et al. 2011; Liu and Chan 2013; Hsu et al. 2014; Xu and Wang 2014; He et al. 2015).

With respect to the TC intensity, it is usually examined in terms of the number of intense typhoons [category 4 and 5 typhoons with a 1-min maximum sustained wind speed greater than 59 m s^{-1}, according to the Saffir–Simpson scale (see www.aoml.noaa.gov/general/lib/laescae.html for a description of the Saffir–Simpson scale)]. Intense typhoons are actually far more destructive than regular TCs due to the higher wind speeds and longer duration of high winds. Therefore, recognizing and comprehending the features of intense typhoon change is of great importance. The intensification of intense typhoons not only shares common environmental preferences with the formation of regular TCs (Chan 2005, 2008; Wang and Zhou 2008) but also requires a favorable storm structure and additional atmospheric/oceanic conditions (Gray 1979; Emanuel 1988, 1999; Frank and Ritchie 2001; Emanuel et al. 2004; Lin et al. 2005, 2008, 2014; Cione et al. 2013). In addition, rapid intensification (RI) is an essential characteristic in intense typhoon development. All category 4 and 5 hurricanes in the North Atlantic (NA) basin (Kaplan and DeMaria 2003) and 90 % of intense typhoons over the WNP (Wang and Zhou 2008) experience at least one RI process in their life cycle, which is closely associated with atmospheric/oceanic dynamical and thermodynamic factors (e.g., Kaplan and DeMaria 2003; Wang and Zhou 2008; Kaplan et al. 2010; Hendricks et al. 2010). Note that the TC formation locations and prevailing tracks also contribute to TC intensity through modulating the duration applied in the intensification (Wu and Wang 2008; Zhao and Wu 2014; Zhao et al. 2014).

From a long-term perspective, Webster et al. (2005) found that the number and proportion of TCs categorized as intense typhoons have increased over the period 1975-2004 in all TC basins. Emanuel (2005) demonstrated a great increase in the power dissipation, which is a combination of the observed intensity, duration, and frequency of TCs, over the WNP and NA basins since the mid-1970s. However, a number of follow-up studies contradicted these findings (e.g., Landsea 2005; Chan 2006, 2008; Landsea et al. 2006; Klotzbach 2006; Kossin et al. 2007; Song et al. 2011; Klotzbach and Landsea 2015) and attributed these inconsistencies to two aspects, i.e., the non-uniformity of the observational quality (Landsea et al. 2006; Wu and Zhao 2012) and discrepancies among available TC best-track datasets (Kamahori et al. 2006; Wu et al. 2006; Kossin et al. 2007; Song et al. 2010). Therefore, utilizing all of the available TC best-track datasets and focusing on the period after the termination of operational aircraft observation, the present study aims to address the following questions. (1) Did intense typhoons exhibit a change similar to regular TCs over the WNP in recent decades? (2) If not, what are the unique features and causes of the intense typhoon change?

To address the aforementioned questions, the remainder of this paper is organized as follows. Section 2 introduces the datasets and methodologies. A comprehensive description of the changes in the intense typhoons during the most recent two decades is presented in Sect. 3. Section 4 investigates the dynamical and thermodynamic factors responsible for the changes of intense typhoons. In Sect. 5, the influences of TCs on the background conditions are examined while the role of the regional SST on the changes of intense typhoons is discussed. In addition, the question why the unusual growth only exhibited in September rather than the other months is investigated in Sect. 5. Finally, a summary is provided in Sect. 6.

2 Datasets and methodologies

2.1 Datasets

Considering the possible inconsistencies among different datasets (Kamahori et al. 2006; Wu et al. 2006; Kossin et al. 2007; Song et al. 2010), we basically retrieved all of the accessible TC best-track datasets for the WNP, i.e., best-track data from the Joint Typhoon Warning Center (JTWC 2015), the Regional Specialized Meteorological Center (RSMC 2015) Tokyo, and the China Meteorological Administration (CMA 2015). To investigate if intense typhoon occurrences experienced similar changes as regular TCs during the most recent two decades, we employed datasets from 1989 to 2012, corresponding to the study period in He et al. (2015). Additionally, the Advanced Dvorak Technique-Hurricane Satellite (ADT-HURSAT) dataset (Kossin et al. 2013), which presently spans the period 1982–2009, was applied to verify our results. The ADT-HURSAT dataset contains more temporally consistent records of TC intensity than other datasets, since a state-of-the-art automated algorithm was applied to globally homogenized satellite data (Knapp and Kossin 2007; Kossin et al. 2007, 2014). Due to similar features obtained from ADT-HURSAT, the results from ADT-HURSAT are not shown here.

In addition, several atmospheric and oceanic variables were examined to understand the influences of the large-scale environment exerted on intense typhoon occurrences over the WNP. These variables are listed as follows: daily

zonal and meridional wind components, vertical velocity, relative vorticity, relative and specific humidity, air temperature and surface pressure from the European Centre for Medium-Range Weather Forecasts (ECMWF) Interim Re-Analysis (ERA-interim) dataset (Dee et al. 2011); daily precipitation from the Global Precipitation Climatology Project (GPCP) version 1.2 (Huffman et al. 2001); daily SST from National Oceanic and Atmospheric Administration (NOAA) Optimum Interpolation SST version 2 (Reynolds et al. 2007); monthly mean ocean temperature from National Centers for Environmental Prediction (NCEP) Global Ocean Data Assimilation System (GODAS) (Behringer and Xue 2004); and daily latent/sensible heat fluxes from Woods Hole Oceanographic Institution (WHOI) Objectively Analyzed air–sea Fluxes (OAFlux) Project (Yu et al. 2008). These aforementioned datasets cover the study period, i.e., from 1989 to 2012, except for GPCP daily precipitation that extends from October 1996 to the present.

2.2 Methodologies

In this study, a TC (intense typhoon) is defined as a system with a maximum sustained 1-min mean surface wind speed of greater than 17.5 (59.0) m s^{-1} during its lifetime. The location of TC (including intense typhoon) formation is defined as the position in which the system first reached tropical storm intensity, i.e., 17.5 m s^{-1}. The TC (intense typhoon) genesis locations are counted for each 5° × 5° grid box over the WNP region (0°–40°N, 100°E–180°). The total count for each grid box is defined as TC (intense typhoon) genesis frequency.

Note that the three best-track datasets adopt different definitions for the maximum sustained wind speed [unit: m s^{-1}; 1-min-averaged (MSW_1) for JTWC, 2-min-averaged (MSW_2) for CMA, and 10-min-averaged (MSW_{10}) for RSMC], which interfered with a unified recognition of the TC intensity, especially for the intensity of intense typhoons. Hence, we adjusted the MSW_{10} (MSW_2) of RSMC (CMA) to MSW_1 as follows, according to Knapp and Kruk (2010).

$$MSW_1 = 1.667(MSW_{10} - 12.0) \tag{1}$$

$$MSW_1 = 1.148MSW_2 \tag{2}$$

To quantitatively identify the dominant factors for TC genesis, the modified version of the genesis potential index (GPI) (Murakami and Wang 2010) in which the vertical motion effect is incorporated into the original GPI formula (Emanuel and Nolan 2004) was used in this study:

$$GPI = \left|10^5\eta\right|^{\frac{3}{2}}\left(\frac{RH}{50}\right)^3\left(\frac{V_{pot}}{70}\right)^3(1+0.1V_s)^{-2}\left(\frac{-\omega+0.1}{0.1}\right) \tag{3}$$

where η is the absolute vorticity (s^{-1}) at 850 hPa, RH is the relative humidity (%) at 700 hPa, V_{pot} is the maximum TC potential intensity (PI; m s^{-1}), V_s is the magnitude of the vertical zonal wind shear (m s^{-1}) between 850 and 200 hPa, and ω is the vertical velocity (Pa s^{-1}) at 500 hPa. The definition of PI is based on work by Emanuel (1995) but modified by Bister and Emanuel (1998) as follows:

$$V_{pot}^2 = \frac{C_k}{C_D}\frac{T_s}{T_0}\left(CAPE^* - CAPE^b\right) \tag{4}$$

where C_k is the exchange coefficient for enthalpy, C_D is the drag coefficient, T_s is the SST (K), and T_0 is the mean outflow temperature (K). $CAPE^*$ is the value of the convective available potential energy (CAPE) of the air lifted from saturation at sea level with reference to the environmental sounding, and $CAPE^b$ is that of the boundary layer air.

In addition, to detect regime shifts in the time series, this study employed the regime detection algorithm developed by Rodionov (2004). The method can identify a significant change in the sequential running means with a certain cutoff length based on Student's t test. In this study, a cutoff length of 7 years was used; only those regime shifts significant at the 95 % significance level or higher were considered in the subsequent analysis.

3 Unusual growth of intense typhoon occurrences over the Philippine Sea in September after the mid-2000s

3.1 Phenomena

Previous study has noticed that TC activity over the WNP during the peak season [July–October (JASO)] experienced a pronounced decadal change in the late 1990s (He et al. 2015). Correspondingly, we were curious about whether a similar change occurred for intense typhoons. As shown in Fig. 1a, the time series of the WNP intense typhoon occurrence number during JASO was examined. According to the regime detection algorithm (Rodionov 2004), a significant shift could be detected from all three best-track datasets in the late 1990s, which was exactly consistent with the change in the basin TC genesis number (He et al. 2015). In contrast to the basin TC genesis number change, the number of intense typhoon occurrences exhibited an unusual increase around the mid-2000s, particularly in the RSMC and CMA datasets. To confirm the abrupt increase in intense typhoon occurrences during the latest 15 years, we examined the change in the number of intense typhoon occurrences in each individual month (July, August, September and October). Based on the regime detection algorithm (Rodionov 2004), a remarkable shift in the intense typhoon occurrences was identified around the mid-2000s

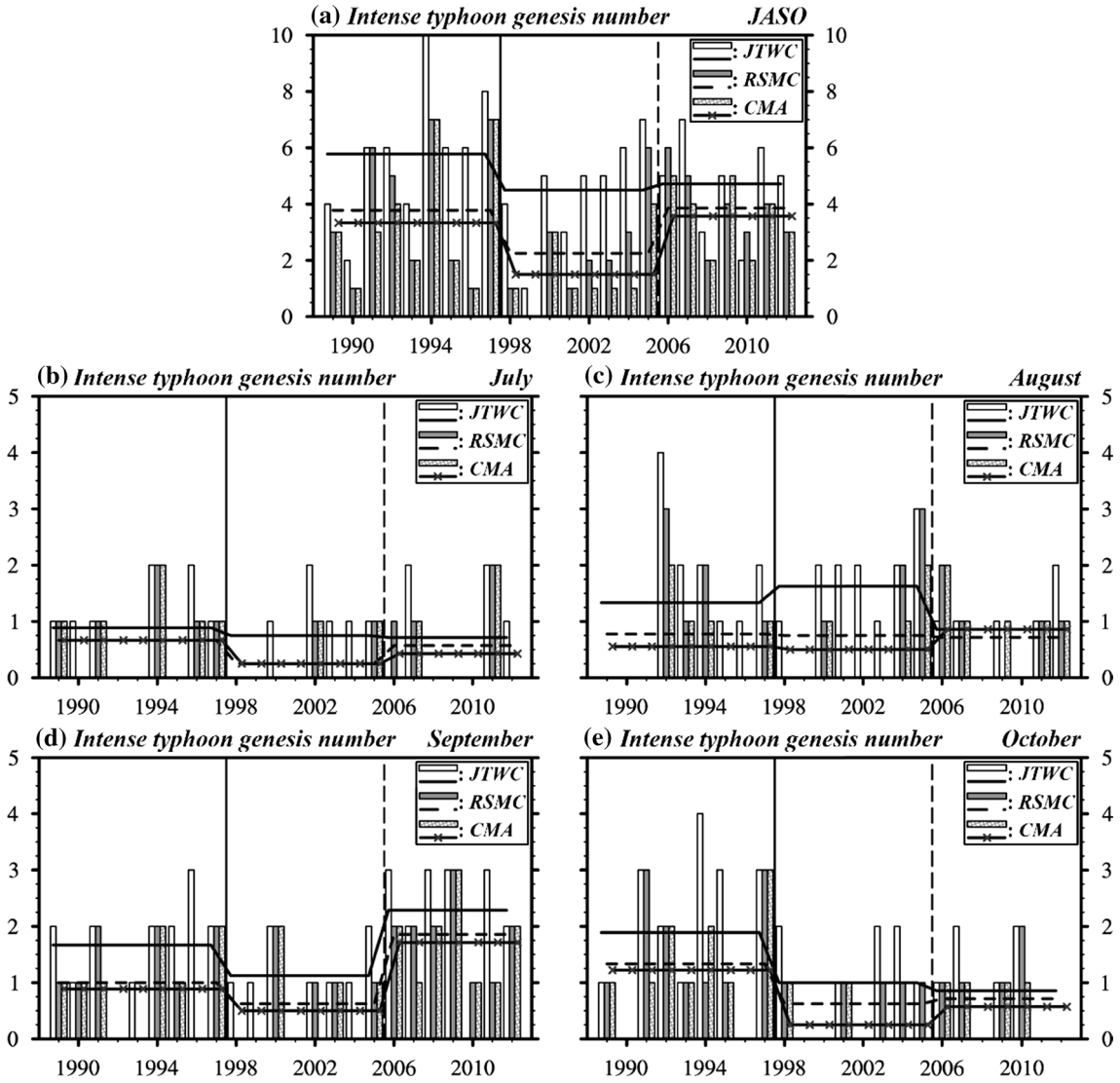

Fig. 1 Time series (*white bars* from JTWC, *gray bars* from RSMC, *stippled bars* from CMA) of the intense typhoon genesis number over the WNP from 1989 to 2012 for **a** the boreal summer (JASO), **b** July, **c** August, **d** September and **e** October. The *vertical lines* divide the period 1989–2012 according to the regime detection algorithm. The *solid vertical line* indicates the regime shift point of the intense typhoon genesis number over the WNP during JASO, whereas the *dashed vertical line* indicates that in September. The *lines* (*solid line* from JTWC, *dashed line* from RSMC, *line with markers* from CMA) indicate the mean in each period

in September from all three datasets (Fig. 1d). Specifically, the number of intense typhoon occurrences increased from 1.1/0.6/0.5 (JTWC/RSMC/CMA) before the mid-2000s (1998-2005) to 2.3/1.9/1.7 (JTWC/RSMC/CMA) after the mid-2000s (2006–2012). However, changes in the number of intense typhoon occurrences in the other three months (July, August and October) were neither consistent among the three datasets nor statistically significant (Fig. 1b, c, e). Therefore, we can safely infer that the increase in intense typhoon occurrences over the WNP after the mid-2000s was mainly attributed to the change in September. For this reason, the following analyses focused on the changes in intense typhoons over the WNP in September between the two periods after the late 1990s divided by the mid-2000s: 1998–2005 (hereafter, P1) and 2006–2012 (hereafter, P2).

Furthermore, we examined the spatial distribution difference of intense typhoon genesis frequency in September for the two periods (Fig. 2a–c). Compared with P1, the most remarkable increase in P2 occurred over the PS (5°–25°N, 125°–140°E; shown as a red rectangle), which is consistently well exhibited in all three datasets. Until the present, the mid-2000s change in the WNP intense typhoon occurrences detected in Fig. 1d primarily occurred over the PS in September. According to the time series of the intense typhoon genesis number over the PS (Fig. 3a), intense typhoons were rarely formed over the PS in September before the mid-2000s, but

the average intense typhoon genesis number reached up to 1.6/1.4/1.3 (JTWC/RSMC/CMA) after the mid-2000s, which is at least statistically significant at the 99 % confidence level.

3.2 Contributory factors

Why did intense typhoon occurrences experience such an unusual increase over the PS in September after the mid-2000s? To answer this question, we examined two potential contributory factors: TC genesis and TC intensification. In terms of TC genesis, the spatial distribution differences between these two periods (P2 − P1) shows that the largest increase of TC genesis frequency occurred over the PS in all three datasets (Fig. 2d–f). As shown in Fig. 3b, the number of TCs formed over the PS also exhibited an abrupt increase after the mid-2000s in all three datasets, although a slight decrease initially occurred after the late 1990s. Among the increment of the TC genesis number from P1 to P2, intense typhoons account for 83.8/115.9/70.6 % (JTWC/RSMC/CMA) of the increment. Thus, there is no doubt that the increased TC genesis was conducive to the abrupt growth of intense typhoon occurrences over the PS.

In addition, to examine whether the percentage of regular TCs developing into intense typhoon increased over the PS in September after the mid-2000s, i.e., if TCs formed over the PS were more likely to develop into intense typhoons, the percentage was defined as the proportion of the number of intense typhoons formed over the PS against the total TC genesis number over the PS. Since no TCs formed over the PS in the several years before the mid-2000s, we calculated the percentage for the two whole periods rather than each individual year. The result shows that the percentage increased from 37.5/14.3/0.0 % (JTWC/RSMC/CMA), before the mid-2000s, to 64.7/71.4/50 % (JTWC/RSMC/CMA), after the mid-2000s, which suggests that the TCs formed over the PS had a greater likelihood of intensifying into intense typhoons during P2.

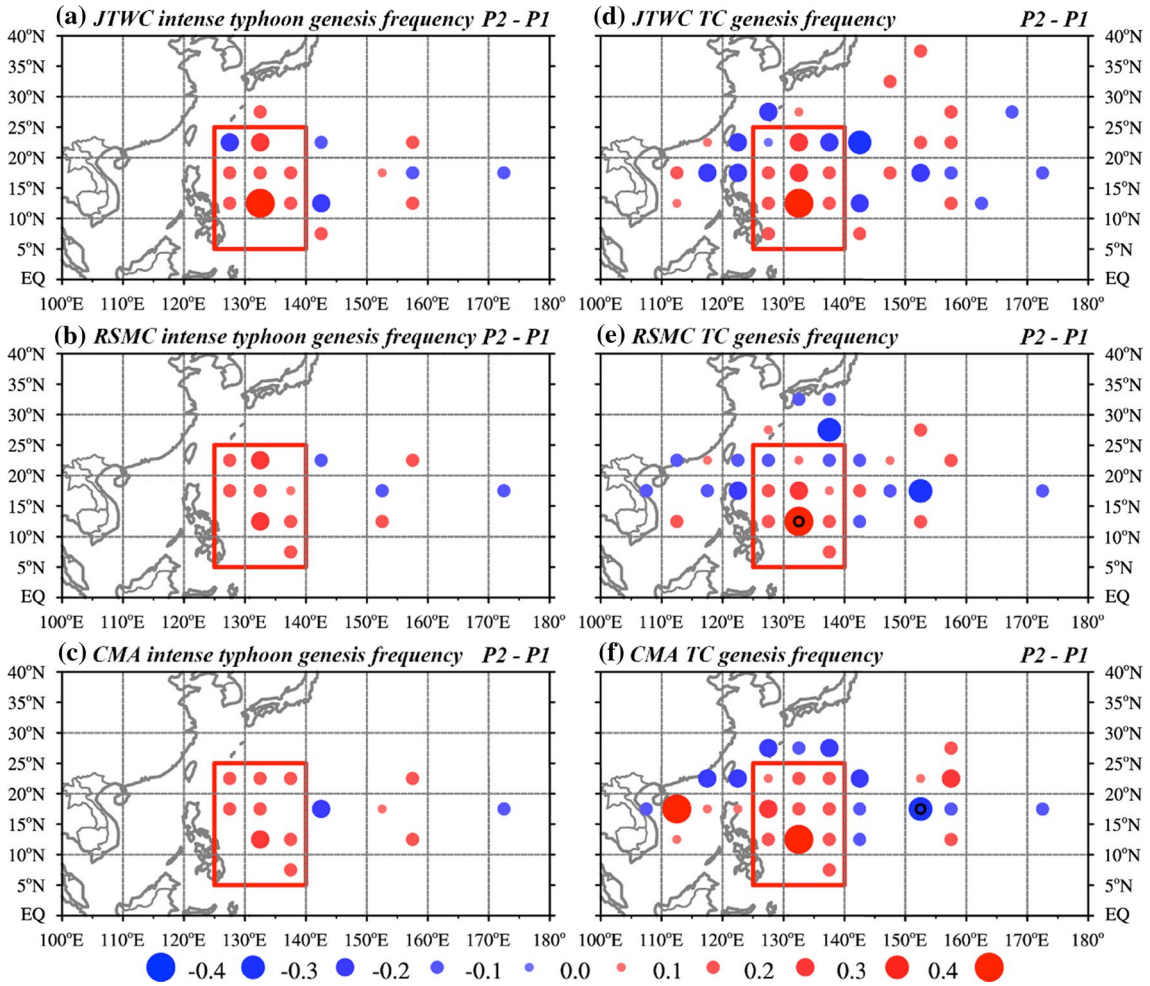

Fig. 2 Differences (P2 − P1) of the intense typhoon genesis frequency (**a**–**c**) and TC genesis frequency (**d**–**f**) in September. Among them, the *first row* (**a**, **d**) is from JTWC, the *second row* (**b**, **e**) is from RSMC, and the *third row* (**c**, **f**) is from CMA. The *black hollow circles* indicate the differences significant at the 90 % confidence level. The *rectangles* show regions with pronounced changes in intense typhoon genesis frequency

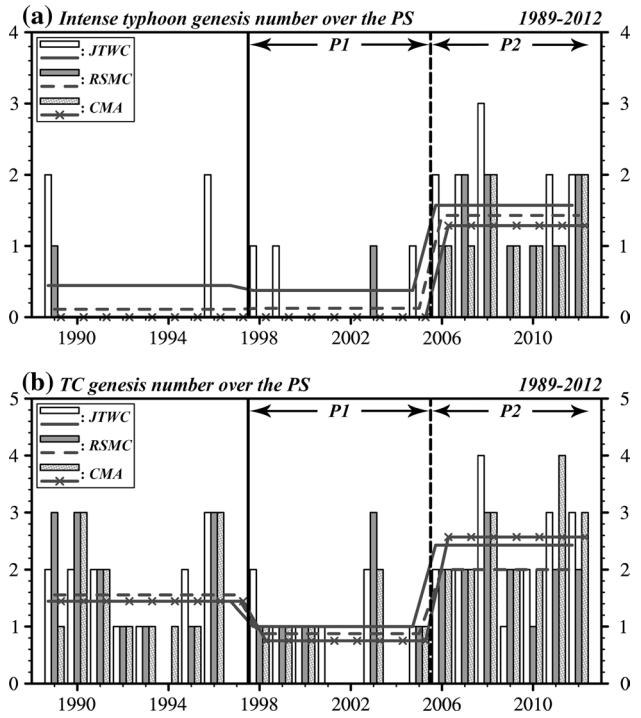

Fig. 3 Time series (*white bars* from JTWC, *gray bars* from RSMC, *stippled bars* from CMA) of the **a** intense typhoon genesis number and **b** regular TC genesis number over the PS in September from 1989 to 2012. The *vertical lines* divide the period of 1989 to 2012 as in Fig. 1. The *lines* (*solid line* from JTWC, *dashed line* from RSMC, *line with markers* from CMA) indicate the mean in each period

To further understand TC intensification, we examined the exact locations of the intense typhoon geneses and intense typhoon lifetime maximum intensity (LMI) occurrences over the WNP during the two periods (shown in Fig. 4). Consequently, an evident southwestward migration of intense typhoon genesis locations was observed in September after the mid-2000s, with the center shifted from east of 140°E to the PS. In addition, the locations of intense typhoon LMI occurrences were also assembled in the extended PS (5°–25°N, 122°–140°E; shown as a purple rectangle with dash line). Comparisons between the two periods in terms of the locations in which intense typhoons formed and reached their LMI reveal that these intense typhoons intensified to their LMI in a shorter distance during P2. Meanwhile, the average duration for the intensification decreased from 3.8/4.0/4.8 days (JTWC/RSMC/CMA) in P1 to 3.2/2.6/3.6 days (JTWC/RSMC/CMA) in P2. Thus, we can infer that the strengthening of these intense typhoons was likely associated with more favorable environmental conditions for TC intensification in P2.

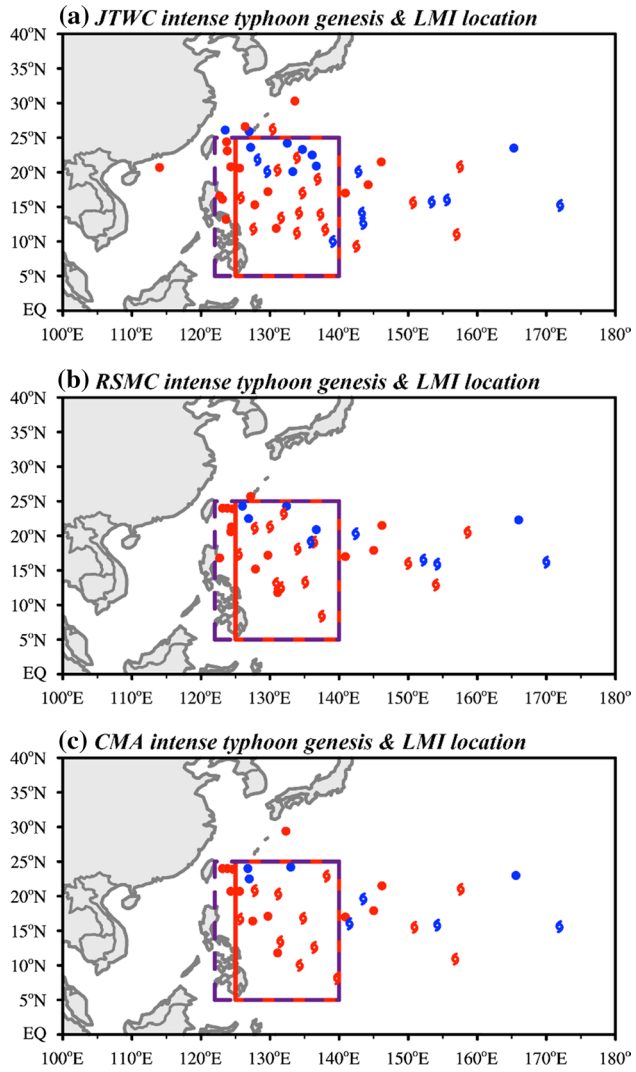

Fig. 4 Locations of intense typhoon genesis and their lifetime maximum intensity (LMI) occurrence in September from **a** JTWC, **b** RSMC and **c** CMA. The *blue* (*red*) *TC markers* and the *blue* (*red*) *dots* represent the genesis location of intense typhoons and the LMI occurrence location of intense typhoons for P1 (P2), respectively. The *red rectangles* show the region with pronounced changes in intense typhoon genesis frequency, corresponding to Fig. 2. The *purple dashed rectangles* show the region in which most of the intense typhoons were enhanced to their LMI in P2

4 Related changes in the environmental dynamical and thermodynamic conditions in the mid-2000s

As previously mentioned, the unusual increase in intense typhoon occurrences over the PS was attributed to the increased TC genesis and more favorable environmental conditions for TC intensification. Here we explore the direct role of the local environmental conditions associated with them.

4.1 TC genesis

In terms of TC genesis, the total change in the GPI in September between the two periods (P2 − P1), as well as the GPI changes obtained by varying each individual GPI element (i.e., varying GPI), was first examined. By taking the logarithm in Eq. (3), the sum of the five varying GPI changes on the right-hand side is identical to the total GPI change. As shown in Fig. 5a, the positive anomalies of GPI and the regular TC genesis frequency (Fig. 2d–f) both appear over the PS, although their maximum centers are not exactly collocated. Regarding individual GPI elements, the results suggest that relative humidity might play a crucial role in the changes of the regular TC genesis over the PS (Fig. 5c). The increased relative humidity (Fig. 5c), combined with the two most important dynamical contributors [i.e., cyclonic vorticity (Fig. 5b) and anomalous ascent (Fig. 5f)], together provided a favorable environment for regular TC genesis over the PS in P2.

Besides that, the spatial distribution difference between the two periods (P2 − P1) within each of the potential dynamical and thermodynamic parameters in GPI was investigated, as shown in Fig. 6. Mostly consistent with the results in Fig. 5, the positive low-level relative vorticity anomalies (Fig. 6a) and anomalous ascent (Fig. 6b) occurred over the PS, along with pronounced 700 hPa wetting anomalies (Fig. 6d) and positive SST anomalies (Fig. 6e), together provided favorable conditions for the development of tropical disturbances over the PS, where regular TC genesis significantly increased in the latest period. In contrast to the warming SST anomalies over the PS, the PI has not shown any significant signals over the PS

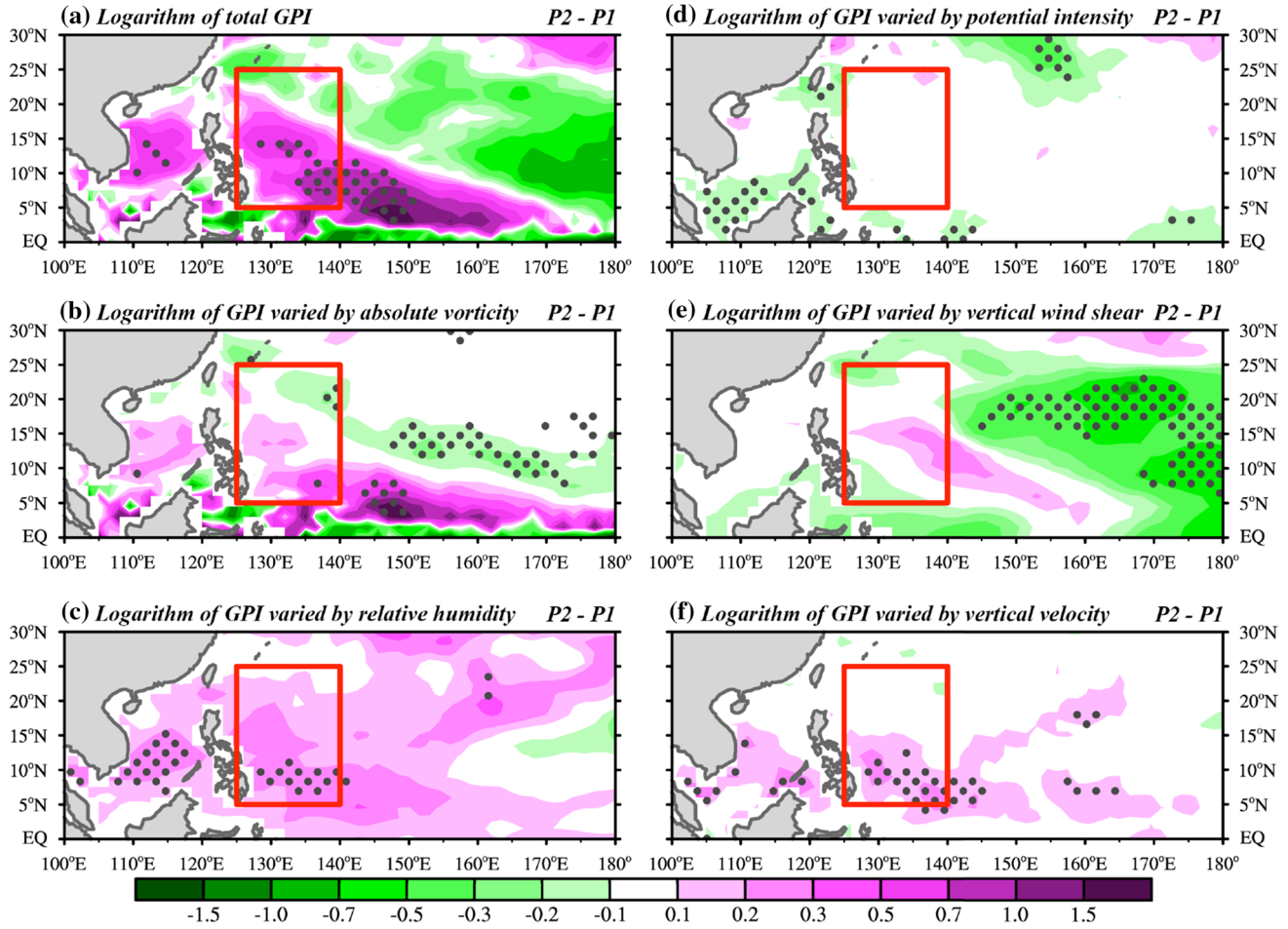

Fig. 5 The difference in the logarithm of **a** the GPI in September between the two periods (P2 − P1), and its changes induced by individual terms: **b** absolute vorticity, **c** relative humidity, **d** potential intensity, **e** vertical wind shear, and **f** vertical velocity. The *dots* mark regions where the differences between the two periods are significant at the 95 % confidence level. The *rectangles* show the region with pronounced changes in intense typhoon genesis frequency, corresponding to Fig. 2

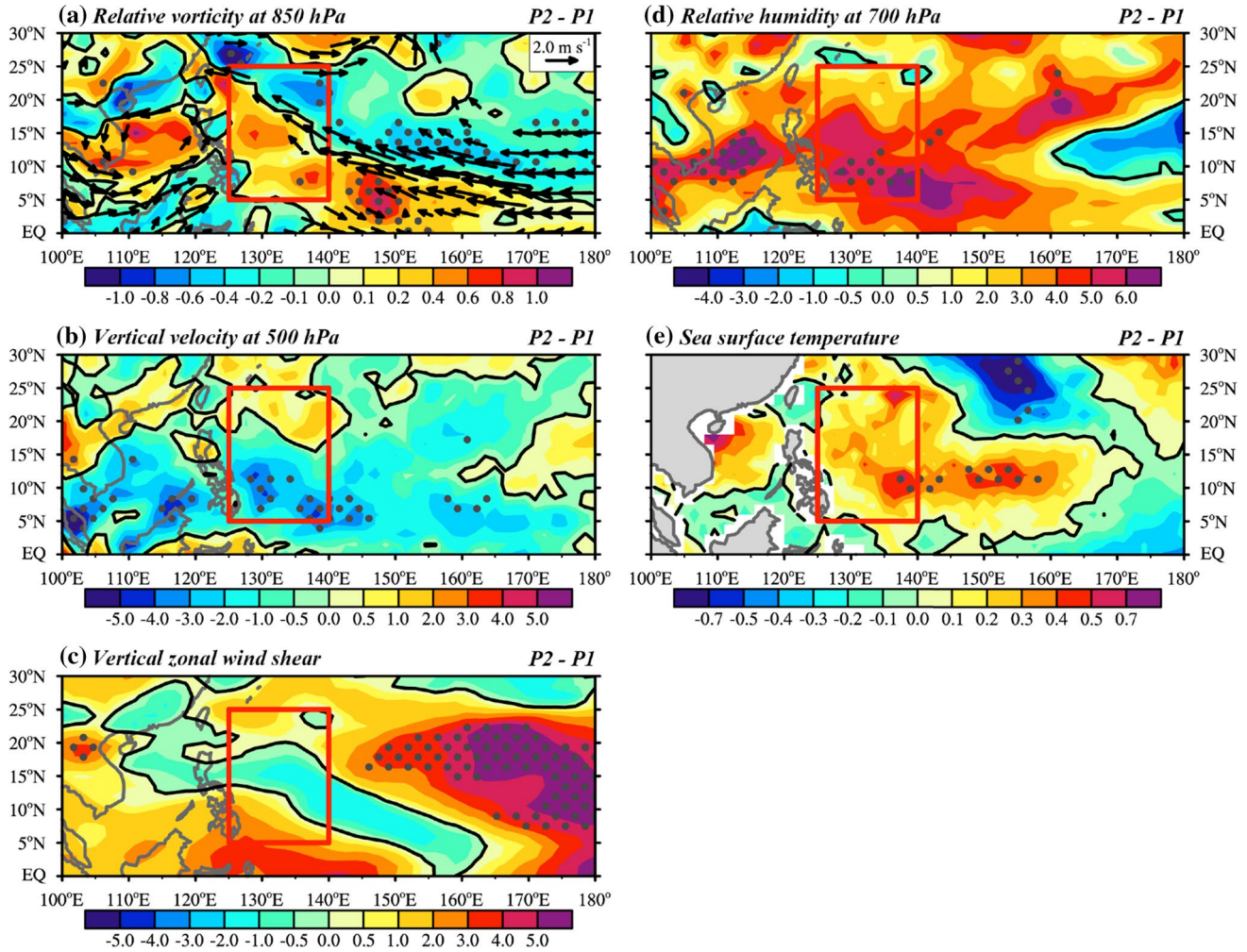

Fig. 6 Changes in the large-scale environment in September (P2 − P1) for **a** 850 hPa relative vorticity (10^{-5} s^{-1}, *shading*) and wind fields (m s^{-1}, *vectors*), **b** 500 hPa vertical velocity (10^{-2} Pa s^{-1}), **c** vertical zonal wind shear (m s^{-1}), **d** 700 hPa relative humidity (%), and **e** sea surface temperature (K). The *thick solid lines* indicate the isolines of zero. The *dots* mark regions where the differences between the two periods are significant at the 95 % confidence level. For the changes of wind fields at 850 hPa in (**a**), only areas where the differences are statistically significant at the 95 % confidence level are shown. The *rectangles* show the region with pronounced changes in intense typhoon genesis frequency, corresponding to Fig. 2

(Fig. 5d), which may be associated with the changes in the mean outflow temperature.

In addition, although relative humidity at 700 hPa exhibited a basin-mode increase, it is worth noting that the largest increase was centered over the South China Sea (SCS) and the PS (Figs. 5c, 6d), exactly coinciding with the cyclonic vorticity anomaly (Figs. 5b, 6a) and anomalous upward motion (Figs. 5f, 6b). Hence, we further investigated the cause for increased relative humidity. As is known, when the specific humidity remains constant and the temperature increases, relative humidity decreases. In this case, because air temperature increases at 700 hPa (not shown), the increase in relative humidity is attributed to the increased specific humidity. To understand the moisture processes resulting in the remarkable increased specific humidity at 700 hPa, the moisture flux and moisture flux convergence (MFC; e.g., Banacos and Schultz 2005) were examined. MFC can be written as

$$\mathrm{MFC} = -\nabla \cdot (q\boldsymbol{V}_h) = -\boldsymbol{V}_h \cdot \nabla q - q\nabla \cdot \boldsymbol{V}_h, \tag{5}$$

$$\mathrm{MFC} = -\mathrm{u}\frac{\partial \mathrm{q}}{\partial \mathrm{x}} - v\frac{\partial q}{\partial y} - q\left(\frac{\partial u}{\partial x} + \frac{\partial v}{\partial y}\right). \tag{6}$$

In Eq. (6), the advection term $(-\mathrm{u}\frac{\partial \mathrm{q}}{\partial \mathrm{x}} - v\frac{\partial q}{\partial y})$ represents the horizontal advection of the specific humidity, whereas the convergence term $[-q(\frac{\partial u}{\partial x} + \frac{\partial v}{\partial y})]$ denotes the product of the specific humidity and horizontal mass convergence. As shown in Fig. 7, the wetting low-level atmosphere mainly resulted from intensified MFC (Fig. 7a), which was mostly contributed from the convergence

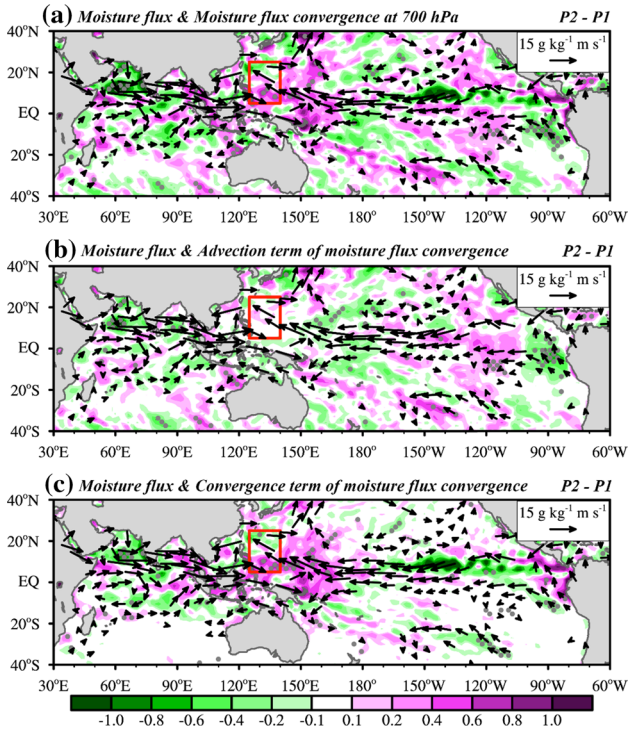

Fig. 7 Changes in **a** moisture flux (g kg^{-1} m s^{-1}, *vectors*) and moisture flux convergence (10^{-5} g kg^{-1} s^{-1}, *shading*), **b** moisture flux (g kg^{-1} m s^{-1}, *vectors*) and the advection term of moisture flux convergence (10^{-5} g kg^{-1} s^{-1}, *shading*), and **c** moisture flux (g kg^{-1} m s^{-1}, *vectors*) and the convergence term of moisture flux convergence (10^{-5} g kg^{-1} s^{-1}, *shading*) in September (P2 − P1). The *dots* mark regions where the differences between the two periods are significant at the 95 % confidence level. The *rectangles* show the region with pronounced changes in intense typhoon genesis frequency, corresponding to Fig. 2

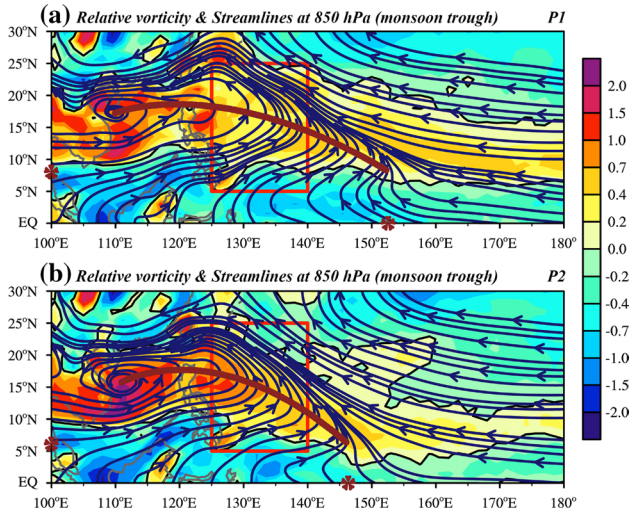

Fig. 8 Relative vorticity (10^{-5} s^{-1}, *shading*) and streamlines at 850 hPa in September for **a** P1 and **b** P2. The *thick solid lines* indicate the isolines of zero. The *brown solid lines* indicate the monsoon trough. The *brown snowflake markers* mark the southern and eastern end of the monsoon trough. The *rectangles* show the region with pronounced changes in intense typhoon genesis frequency, corresponding to Fig. 2

term (Fig. 7c). Because the convergence term is greatly affected by dynamical factors, these results suggest that dynamical variations (i.e., low-level relative vorticity and mid-level vertical velocity) played an essential role in causing the increased TC genesis over PS during P2 rather than thermodynamic factors. Additionally, although relative humidity exhibited similar but a little weaker increase while dynamical factors remained constant in the other three months (not shown), regular TC genesis frequency showed barely any significant change. These results are consistent with previous studies, which proposed that dynamical factors are paramount contributory terms in the regular TC genesis change (Liu and Chan 2013; Hsu et al. 2014; He et al. 2015).

The associated large-scale circulation difference between the two periods (P2 − P1) is manifested in the difference of the monsoon trough. Specifically, we noticed a sickle shaped low-level cyclonic anomaly occurred over the PS (Fig. 6a), which corresponded to the aforementioned positive low-level relative vorticity and ascent over the PS. These changes suggest a southwestward shift and strengthening of the monsoon trough (Fig. 8a, b). Consequently, the PS was mainly located in the strengthened monsoon trough region. According to previous studies, the monsoon trough is an important large-scale circulation system that could provide favorable dynamical and thermodynamic large-scale conditions for TC formation (e.g., Gray 1968, 1975; Ramage 1974; Frank 1987; Holland 1995; Lander 1996; Briegel and Frank 1997; Ritchie and Holland 1999; Chia and Roplewski 2002; Chen et al. 2006; Zong and Wu 2015).

4.2 TC intensification

As mentioned above, the enhanced TC intensification tendency over the extended PS is likely associated with the more favorable environmental conditions for TC intensification. According to previous studies (e.g., Kaplan and DeMaria 2003; Wang and Zhou 2008; Kaplan et al. 2010; Hendricks et al. 2010), TC intensification is influenced by the following factors: relative vorticity at 850 hPa (VOR), vertical velocity at 500 hPa (Omega), vertical zonal wind shear (VWS), divergence at 200 hPa (D200), air temperature at 200 hPa (T200), relative humidity at 700 hPa (RH), SST, available enthalpy (AE; sensible + latent heat flux), depth of the 26 °C isotherm (D26) and tropical cyclone heat potential (TCHP). Therefore, we examined the area-averaged time series of each potential factor over the extended PS in September in both inter-annual and inter-decadal

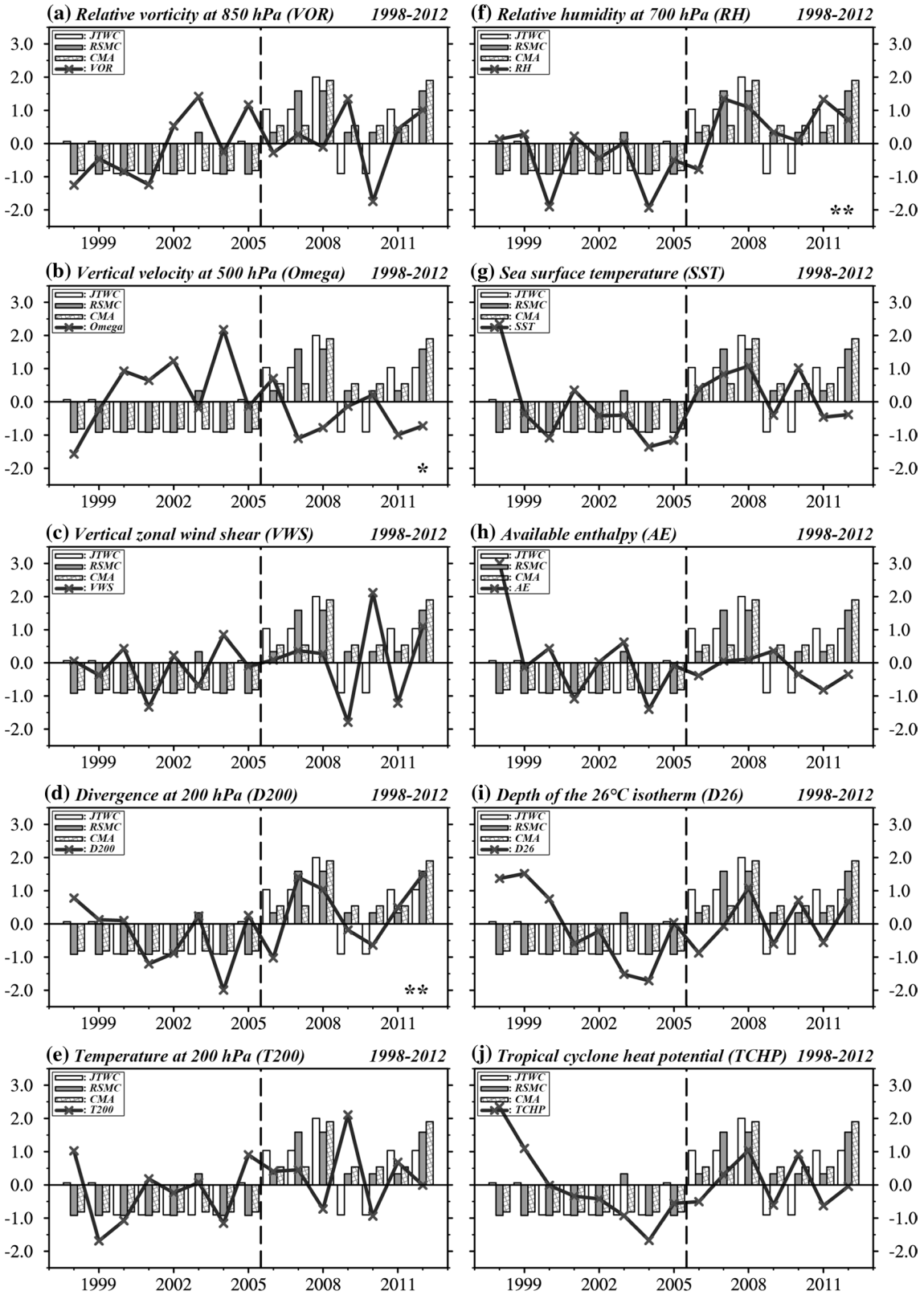

Fig. 9 Time series of **a** VOR, **b** Omega, **c** VWS, **d** D200, **e** T200, **f** RH, **g** SST, **h** AE, **i** D26 and **j** TCHP averaged over the extended PS (5°–25°N, 122°–140°E) in September from 1998 to 2012. All changes are normalized by their own standard deviations. The *bars* are the same as in Fig. 1d, except normalized by their own standard deviations. The *vertical lines* divide the period of 1998 to 2012 as in Fig. 1. The *symbols* "**" and "*" represent the correlation coefficient between the predictor and normalized intense typhoon genesis number significant above the 95 and 90 % confidence level, respectively

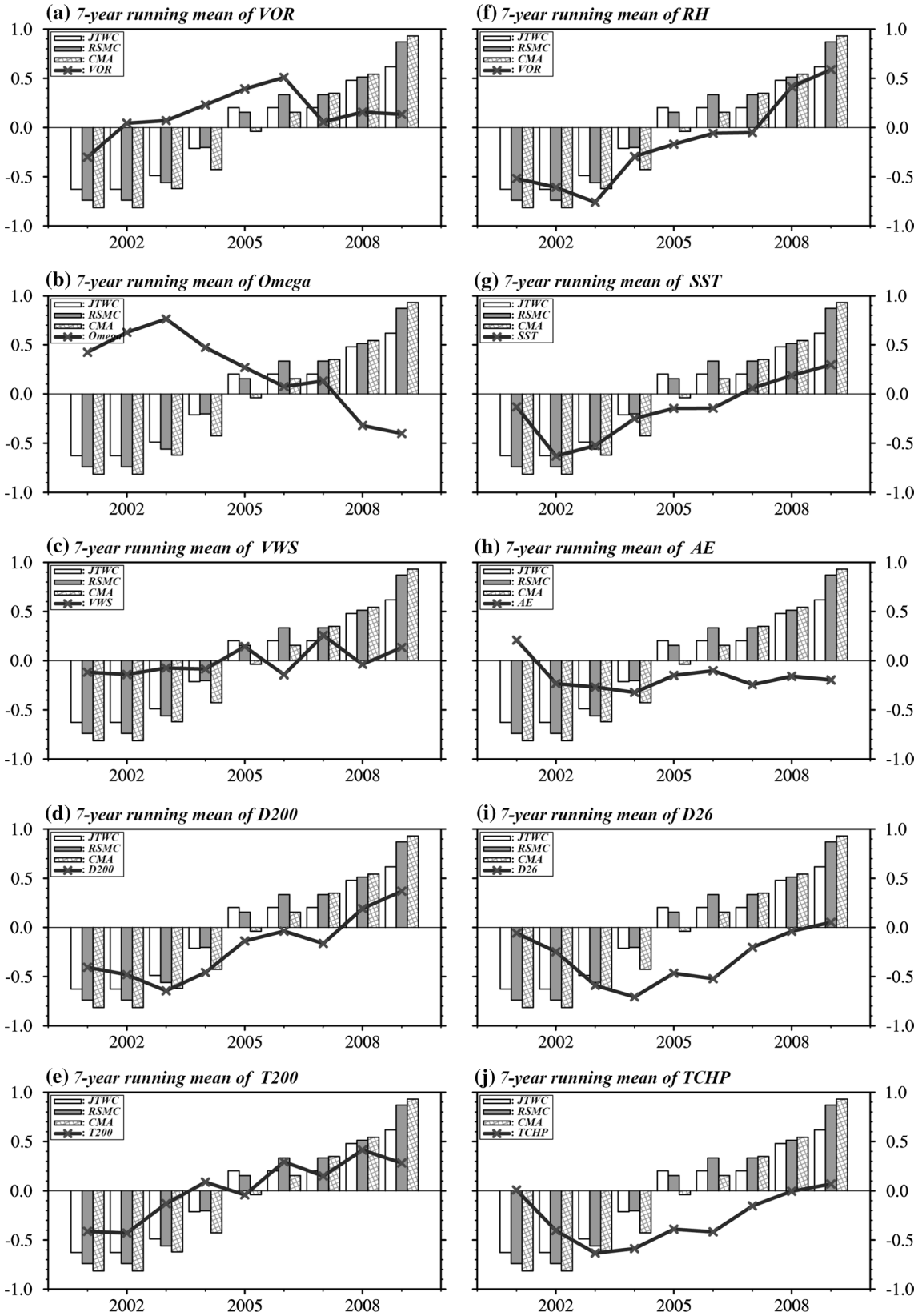

Fig. 10 Same as Fig. 9, except for 7-year running mean

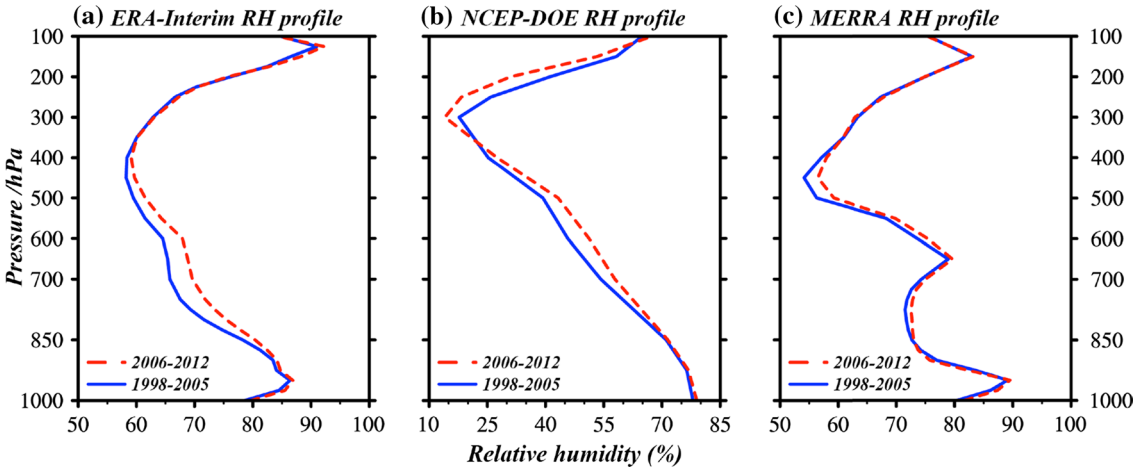

Fig. 11 Profile of relative humidity averaged over the extended PS (5°–25°N, 122°–140°E) in September for P1 (*blue solid line*) and P2 (*red dashed line*) from **a** ERA-interim, **b** NCEP-DOE and **c** MERRA

timescales (Figs. 9, 10). Note that all of the variables shown in Figs. 9 and 10 have been normalized by their own standard deviation. It is clear that the Omega and D200 suddenly became more favorable for TC intensification around the mid-2000s by enhancing ascending motion and upper-level divergence (Fig. 9b, d). Meanwhile, two large-scale thermodynamic variables (i.e., RH and SST) also exhibit sharp increases (Fig. 9f, g) after mid-2000s, which provided an improved thermodynamic large-scale environment over the extended PS for TC intensification in September. These related factors are nicely collocated with the number of intense typhoon occurrences over the PS in September at inter-decadal timescale (Fig. 10b, d, f, g). Among the above-mentioned related factors, RH exhibited the highest correlation with the number of intense typhoon occurrences over the PS in September, with a correlation coefficient of 0.58/0.65/0.57 (JTWC/RSMC/CMA) during the period 1998–2012 in inter-annual timescale. This implies that the increased moisture in the lower troposphere might be more important for inducing the unusual increase in the intense typhoon occurrences in September than the other factors.

To validate the variability of RH, we further examined the difference of the RH vertical profile between the two periods. The result shows that the evident increase of RH uniformly occurred in the lower- and mid- troposphere (from 850 to 400 hPa) in the ERA-interim (Fig. 11a). Besides that, the other two datasets [NCEP-DOE (Kanamitsu et al. 2002) and MERRA (Rienecker et al. 2011)] were applied to verify this result as well. As shown in Fig. 11b, c, similar increases were exhibited in both two datasets, except that the increase occurred in the MERRA dataset was relatively slight. The increase in lower- and mid-tropospheric RH can provide favorable conditions for TC intensification, which might be the dominant contributor to the intense typhoon change of the mid-2000s. The crucial role of lower- and mid-tropospheric RH on TC intensification has also been reported in several previous studies of TC intensification (e.g., Kaplan and DeMaria 2003; Emanuel et al. 2004; Hendricks et al. 2010; Kaplan et al. 2010; Wu et al. 2012).

5 Discussion

5.1 Possible effect of tropical Indo-Pacific SST anomalies

To explore the cause of the aforementioned changes in the environmental conditions and circulations around the mid-2000s, we examined the SST differences between the two periods. As we know, the intense TC wind inevitably mixes the colder subsurface water to the surface, thus cooling local SST (Price 1981; Price et al. 1994; Emanuel 1999; Bender and Ginis 2000; Emanuel et al. 2004; Cione and Uhlhorn 2003; Lin et al. 2013). Considering the so-called cooling effect of TCs on SST (Price 1981; Price et al. 1994; Bender and Ginis 2000), it is necessary to remove the TC effect from the background condition when we attempt to examine the influence that SST exerts on TCs. Here, our strategy for eliminating TC effects is to remove the TC potential affected area within its effective radius, which is defined as 10 degrees from the TC center according to previous studies (Chavas and Emanuel 2010; Lin et al. 2015). As shown in Fig. 12a, evident warming occurred over the tropical WNP and the tropical eastern Pacific in P2 relative to P1, accompanied with an apparent cooling over the tropical central Pacific. Meanwhile, an Indian Ocean Dipole (IOD) like pattern change over the Indian Ocean

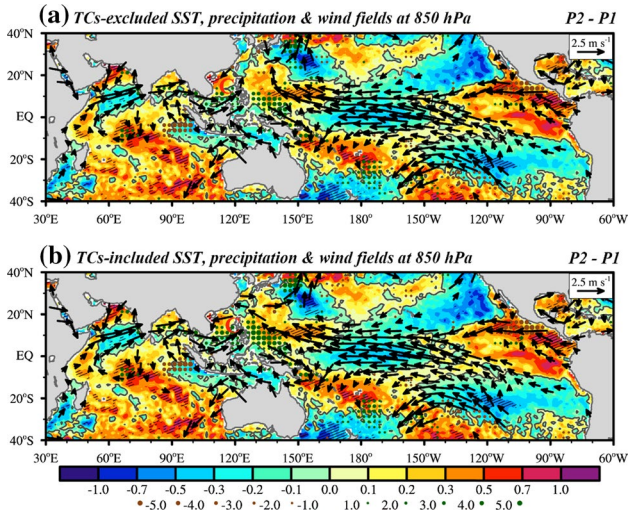

Fig. 12 Changes in the sea surface temperature (SST; K, *shading*), precipitation (mm day^{-1}, *dots*) and 850 hPa wind fields (m s^{-1}, *vectors*) in September (P2 − P1) in two scenarios: **a** TCs-excluded and **b** TCs-included. The *thick solid lines* indicate the isolines of zero in the SST difference. The *stippling* marks region where the SST difference between the two periods is statistically significant at the 95 % confidence level. For the changes in the precipitation and wind fields at 850 hPa, only areas over oceans where the differences are statistically significant at the 95 % confidence level are shown. The "C" indicates the centers of the cyclonic anomalies

was detected with remarkable warming over the southwest Indian Ocean, along with cooling off the Sumatra-Java coast after the mid-2000s.

Furthermore, the influence of SST changes on precipitation and large-scale circulation was examined. As is already known, TCs can not only induce heavy precipitation but also contribute significantly (exceeding 50 % in certain regions) to the seasonal mean of the large-scale circulation (Hsu et al. 2008). Considering the numerous TCs that occurred over the PS, we wondered if the favorable large-scale circulation background resulted from TCs or latent heat released via TC rainfall. Hence, an identical process was applied for the precipitation and 850 hPa wind fields to remove TC effects. The results show that the pattern of precipitation change was almost in agreement with that of the SST change (also shown in Fig. 12a). We noticed that the most significant precipitation changes occurred over the South China Sea–Philippine Sea (SCS–PS), the central tropical southern Indian Ocean and the tropical eastern Pacific. According to Gill (1980), the dynamical linkage between SST, precipitation and large-scale circulation changes was fairly clear. First, the warming over the tropical WNP was conducive to convection, thus increasing precipitation over the SCS–PS. The positive precipitation anomalies could directly generate cyclonic anomalies by the northwestward emanation of ascending Rossby waves. The positive precipitation anomalies also could emanate a warm equatorial Kelvin wave to the east in the troposphere, resulting in an atmospheric anticyclonic anomaly. Second, the cooling over west of Sumatra Island suppressed local convection, which could stimulate the cyclonic anomaly over the SCS–PS by inducing an eastward cool equatorial Kelvin wave. Meanwhile, the negative precipitation anomaly combined with the increased precipitation over the SCS–PS constituted a contrasting rainfall change, potentially inducing equatorial asymmetric heating in the Indo-Pacific Warm Pool area. The equatorial asymmetric heating can induce anomalous cross-equatorial flow, further enhancing the cyclonic anomaly over the SCS–PS. Third, the warming around the central tropical southern Indian Ocean could cause enhanced convection, emanating ascending Rossby waves to the west, resulting in an atmospheric cyclonic anomaly, enhancing the Somali Jet and inducing a remarkable westerly anomaly over South Asia. As a result, the SCS–PS cyclonic anomalies, the South Asian westerly anomalies and the easterly anomalies with anomalous anticyclonic circulation east of the PS together enhanced MFC over the PS, increasing the specific humidity in the lower to middle troposphere over the PS. In contrast, although the cause of the negative precipitation anomaly over the tropical eastern Pacific remains obscure, the suppressed precipitation was consistent with the anomalous anticyclonic circulation over east of the tropical eastern Pacific. Numeric experiments need to be performed to explore the above physical processes in our future work.

So far we have demonstrated that, without involving TCs, SST patterns and the induced precipitation and circulation patterns were favorable for enhancing the moisture flux convergence over the PS, which was beneficial to TC genesis and intensification. Then we further questioned what would happen when TCs get involved. Therefore, we compared the changes in the SST, precipitation and wind fields between the scenarios with and without TCs, as shown in Fig. 12a, b. The results show that the SST changes are similar between these two scenarios, but the precipitation and circulation exhibit some differences. For example, we noticed a northward expansion of the SCS–PS positive precipitation anomaly, which suggests that TC rainfall greatly contributed to the positive precipitation anomaly over the northern SCS–PS. Additionally, the SCS–PS cyclonic anomalies and the anomalous anticyclonic circulation east of the PS are both enhanced after involving TCs. The above results suggest that TC involvement potentially exerted a positive feedback on the anomalous cyclonic circulation over the SCS–PS and the anticyclonic anomalies east of the PS through generating heavy rainfall, ultimately further promoting TC genesis and intensification over the PS.

Considering the potential TC effect on the background conditions, we also re-examined the above-mentioned

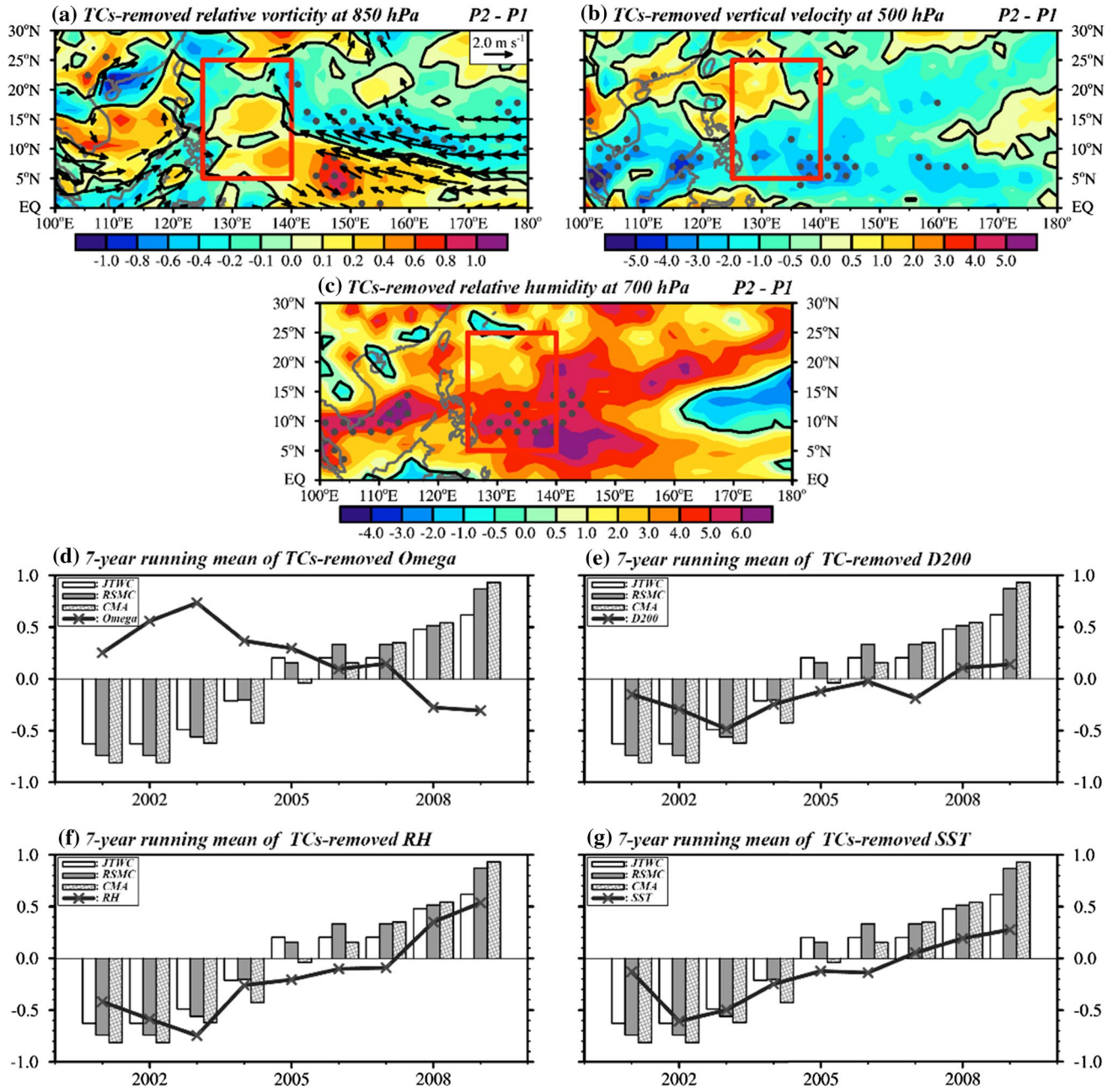

Fig. 13 Changes in the large-scale environment in September (P2 − P1) for TC-removed **a** 850 hPa relative vorticity (10^{-5} s^{-1}, *shading*) and wind field (m s^{-1}, *vectors*), **b** 500 hPa vertical velocity (10^{-2} Pa s^{-1}) and **c** 700 hPa relative humidity (%), and the 7-year running mean of TC-removed **d** Omega, **e** D200, **f** RH, and **g** SST averaged over the extended PS (5°–25°N, 122°–140°E) in September from 1998 to 2012. The *thick solid lines* in (**a**–**c**) indicate the isolines of zero. The *dots* in (**a**–**c**) mark regions where the differences between the two periods are significant at the 95 % confidence level. For the wind field changes at 850 hPa in (**a**), only areas where the differences are statistically significant at the 95 % confidence level are shown. The *rectangles* in (**a**–**c**) show the region with pronounced changes in intense typhoon genesis frequency, corresponding to Fig. 2. All changes in (**d**–**g**) are normalized by their own standard deviations. The *bars* in (**d**–**g**) are the same as in Fig. 1d, except normalized by their own standard deviations

favorable conditions (i.e., relative vorticity, vertical velocity, divergence, relative humidity, and SST) for intense typhoon occurrences (Figs. 6a, b, d, 9b, d, f, g, 10b, d, f, g) after removing TC effects. The results show that the increase in the lower-middle level of the relative humidity remained almost the same, although the increases (decreases) in the local relative vorticity (vertical velocity) were slightly weaker without involving TCs (Fig. 13a–c). Similar phenomena are also displayed in the time series of the key variables without TC effects at inter-annual (not shown) and inter-decadal

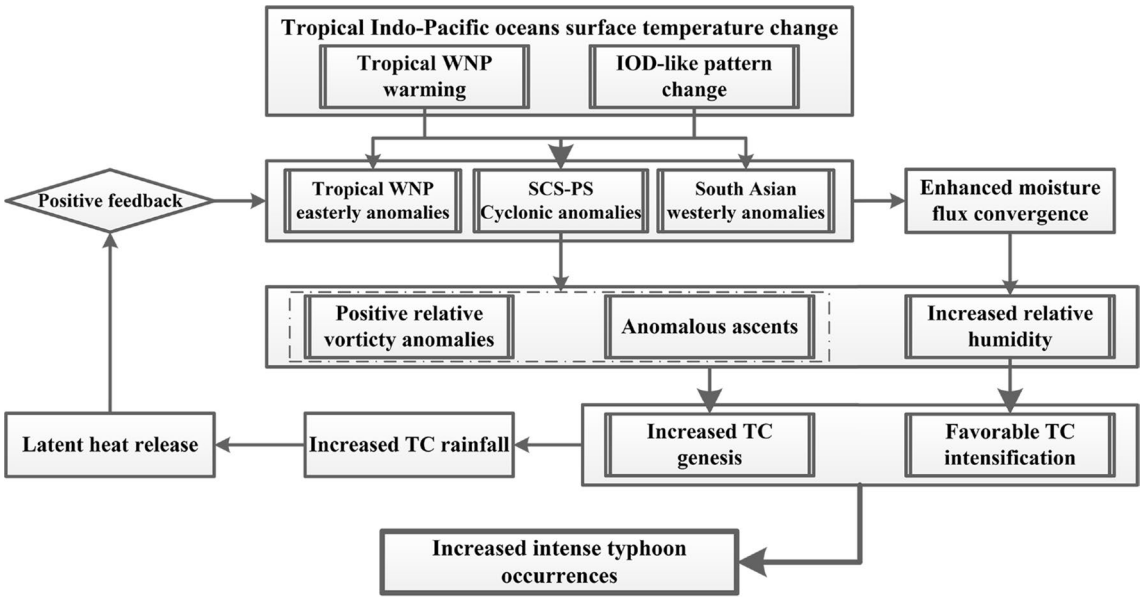

Fig. 14 Schematic diagram summarizing the detailed unusual change in intense typhoon occurrence over the PS, the related causes and its linkage with tropical Indo-Pacific SST changes in the mid-2000s

timescales (Fig. 13d–g). The correlations (matching) between dynamical factors and intense typhoon genesis number at inter-annual (inter-decadal) timescales were reduced, whereas the correlations (matching) between the thermodynamic factors and intense typhoon genesis number maintained the same level. The above results confirm the appreciable contribution of TCs on large-scale circulation (i.e., dynamical factors). They also further emphasize the essential role of the thermodynamic background conditions (i.e., relative humidity and SST) on TC intensification.

5.2 Why was the remarkable increase of intense typhoon occurrences only exhibited in September?

An unsolved question is why the remarkable increase of intense typhoon occurrences was only exhibited in September. As previously mentioned, relative humidity exhibited similar but a little weaker increase whereas relative vorticity (vertical velocity) did not show any significant increase (decrease) in the other three months, which could not be able to provide favorable dynamical conditions for the increase of TC genesis. Further examination found it was because of barely any significant cyclonic anomalies appeared over the SCS–PS region, although warming SST anomalies also occurred over the tropical WNP in July and August (not shown). Then the question arises: why did the tropical WNP warming SST anomalies have caused the favorable dynamical condition in September rather than in July and August? Herein, three possible reasons are proposed. First, the local summer rainfall over the PS, the SCS, and the Bay of Bengal are significantly negatively correlated with SST anomalies, which means the local SST is primarily forced to respond passively to the atmosphere during summer wet season (e.g., Wang et al. 2004). The major process is that the decreased rainfall and cloudiness will tend to increase the downward solar radiation into the ocean, thus resulting in a warmer local SST. Conversely, the correlation between SST and precipitation turns to be positive in September, which indicates that the SST change becomes a dominant driving factor in air–sea interaction, i.e., a warming SST could increase the local rainfall through enhancing the local convection. Second, according to the seasonal march of the Asian-Pacific summer monsoon (Wang and Lin 2002), the monsoon retreats from the SCS–PS region in early September. As a result, the SCS–PS region experiences a transition from wet season to dry season in early September and the rainfall exhibits a sharp decrease over the SCS–PS in September, which could be the major reason for the above-mentioned contrasting change in the simultaneous SST-rainfall correlation from July/August to September. Third, the IOD-like pattern was most significantly exhibited in September, which was just consistent with the IOD event peak season (Saji et al. 1999). Naturally, the IOD-like pattern exerted the most remarkable effect on the SCS–PS cyclonic anomaly in September.

6 Summary

All three best-track datasets demonstrated an unusual increase in intense typhoon occurrences over the PS in September after the mid-2000s during the global warming hiatus period (1998–present). Specifically, intense typhoons rarely

occurred over the PS in September before the mid-2000s, with a frequency of fewer than 0.4 per year. However, the number reached up to nearly 1.5 per year after the mid-2000s.

The abrupt increase in intense typhoon occurrences over the PS mainly resulted from the increased TC genesis and more favorable environmental conditions for TC intensification. The increased TC genesis was primarily associated with anomalous local dynamical conditions (i.e., low-level vorticity and vertical velocity), which corresponded to a southwestward shift and strengthening of the monsoon trough. Additionally, the enhanced TC intensification tendency was mainly attributed to the favorable thermodynamic large-scale conditions. Thereinto, the increased relative humidity that resulted from intensified moisture flux convergence exerted essential effect on the TC intensification.

The aforementioned changes in the environmental conditions and circulation were closely linked with the changes in tropical Indo-Pacific SST, since the boundary SST anomalies turn to be a dominant factor in air–sea interaction in September. Both the tropical WNP warming and the IOD-like pattern changes over the Indian Ocean were considered to play essential roles in inducing the SCS–PS cyclonic anomaly and the associated dynamical conditions that favored TC genesis over the PS. The anomalous cyclonic circulation over the SCS–PS, combined with westerly (easterly) anomalies over the western (eastern) flank of the SCS–PS, together enhanced MFC over the PS, thus increasing the relative humidity in the lower to middle levels of the troposphere, promoting TC intensification over the PS. In addition, TCs potentially exerted a positive feedback on the anomalous cyclonic circulation over the SCS–PS and the anticyclonic anomalies east of the PS by generating heavy rainfall, ultimately further promoting TC genesis and intensification over the PS. Finally, we provided a schematic diagram to summarize the unusual change in intense typhoon occurrences over the PS, the related causes and its linkage with tropical Indo-Pacific SST changes in the mid-2000s (Fig. 14).

Acknowledgments The authors are grateful to Dr. Bo Wu for his constructive comments. This study was financially supported by the National Basic Research Program ('973' Program) of China (Grant No. 2012CB955401) and the National Natural Science Foundation of China (Grant Nos. 41375003 and 41321001). BW acknowledges the support from Climate Dynamics Program of the National Science Foundation under award No NOAA/DYNAMO # NA13OAR4310167 and the National Research Foundation (NRF) of Korea through a Global Research Laboratory (GRL) grant (MEST, #2011-0021927). This is the ESMC publication 110.

References

Banacos PC, Schultz DM (2005) The use of moisture flux convergence in forecasting convective initiation: historical and operational perspectives. Weather Forecast 20:351–366

Behringer DW, Xue Y (2004) Evaluation of the global ocean data assimilation system at NCEP. In: The Pacific Ocean. Eighth symposium on integrated observing and assimilation system for atmosphere, ocean, and land surface, AMS 84th annual meeting, Washington State Convention and Trade Center, Seattle, Washington, DC, pp 11–15

Bender MA, Ginis I (2000) Real-case simulations of hurricane–ocean interaction using a high-resolution coupled model: effects on hurricane intensity. Mon Weather Rev 128:917–946

Bister M, Emanuel KA (1998) Dissipative heating and hurricane intensity. Meteorol Atmos Phys 65:233–240. doi:10.1007/BF01030791

Briegel LM, Frank WM (1997) Large-scale influences on tropical cyclogenesis in the western North Pacific. Mon Weather Rev 125:1397–1413

Chan JCL (2005) Interannual and interdecadal variations of tropical cyclone activity over the western North Pacific. Meteorol Atmos Phys 89:143–152

Chan JCL (2006) Comments on ''Changes in tropical cyclone number, duration, and intensity in a warming environment''. Science 311:1713b

Chan JCL (2008) Decadal variations of intense typhoon occurrence in the western North Pacific. Proc R Soc Lond 464A:249–272

Chavas DR, Emanuel KA (2010) A QuikSCAT climatology of tropical cyclone size. Geophys Res Lett 37:L18816. doi:10.1029/2010GL044558

Chen TC, Wang SY, Yen MC (2006) Interannual variation of the tropical cyclone activity over the western North Pacific. J Clim 19:5709–5720

Chia HH, Roplewski CF (2002) The interannual variability in the genesis location of tropical cyclones in the northwest Pacific. J Clim 15:2934–2944

Cione JJ, Uhlhorn EW (2003) Sea surface temperature variability in hurricanes: implications with respect to intensity change. Mon Weather Rev 131:1783–1796

Cione JJ, Kalina EA, Zhang JA, Uhlhorn EW (2013) Observations of air–sea interaction and intensity change in hurricanes. Mon Weather Rev 141:2368–2382

CMA (2015) China Meteorological Administration Tropical Cyclone Data Center western North Pacific best track data. http://tcdata.typhoon.gov.cn/en/zjljsjj_zlhq.html

Dee D et al (2011) The ERA-Interim reanalysis: configuration and performance of the data assimilation system. Q J R Met Soc 137:535–597

Emanuel KA (1988) The maximum intensity of hurricanes. J Atmos Sci 45:1143–1155

Emanuel KA (1995) Sensitivity of tropical cyclones to surface exchange coefficients and a revised steady-state model incorporating eye dynamics. J Atmos Sci 52:3969–3976

Emanuel KA (1999) Thermodynamic control of hurricane intensity. Nature 401:665–669. doi:10.1038/44326

Emanuel KA (2005) Increasing destructiveness of tropical cyclones over the past 30 years. Nature 436:686–688

Emanuel KA, Nolan DS (2004) Tropical cyclone activity and global climate. Preprints, 26th conference on hurricanes and tropical meteorology, Miami, FL. American Meteorological Society, pp 240–241

Emanuel KA, DesAutels C, Holloway C, Korty R (2004) Environmental control of tropical cyclone intensity. J Atmos Sci 61:843–858

Frank WM (1987) Tropical cyclone formation. In: Elsberry RL, Frank WM, Holland GJ, Jarell JD, Southern RL (eds) A global view of tropical cyclones. Naval Postgraduate School, Monterey, pp 53–90

Frank WM, Ritchie EA (2001) Effects of vertical wind shear on the intensity and structure of numerically simulated hurricanes. Mon Weather Rev 129:2249–2269

Gill AE (1980) Some simple solutions for heat-induced tropical circulation. Q J R Meteorol Soc 106:447–462

Gray WM (1968) Global view of the origin of tropical disturbances and storms. Mon Weather Rev 96:669–700

Gray WM (1975) Tropical cyclone genesis. Departmentt of Atmospheric Science, Paper No. 232, Colorado State University, Ft. Collins, CO, 121 pp

Gray WM (1979) Hurricanes: their formation, structure and likely role in the tropical circulation. In: Shaw DB (ed) Meteorology over the tropical oceans. Royal Meteorological Society, Berkshire, pp 155–218

He H, Yang J, Gong D-Y, Mao R, Wang Y, Gao MN (2015) Decadal changes in tropical cyclone activity over the western North Pacific in the late 1990s. Clim Dyn 45:3317–3329. doi:10.1007/s00382-015-2541-1

Hendricks EA, Peng MS, Fu B, Li T (2010) Quantifying environmental control on tropical cyclone intensity change. Mon Weather Rev 138:3243–3271

Holland GJ (1995) Scale interaction in the western Pacific monsoon. Meteorol Atmos Phys 56:57–79

Hong CC, Wu YK, Li T, Chang CC (2014) The climate regime shift over the Pacific during 1996/1997. Clim Dyn 43:435–446

Hsu H-H, Hung C-H, Lo A-K, Wu C-C, Hung C-W (2008) Influence of tropical cyclones on the estimation of climate variability in the tropical western north Pacific. J Clim 21:2960–2975

Hsu PC, Chu PS, Murakami H, Zhao X (2014) An abrupt decrease in the late-season typhoon activity over the western North Pacific. J Clim 27:4296–4312

Huffman GJ, Adler RF, Morrissey MM, Bolvin DT, Curtis S, Joyce R, McGavock B, Susskind J (2001) Global precipitation at one-degree daily resolution from multi-satellite observations. J Hydrometeor 2:36–50

JTWC (2015) The Joint Typhoon Warning Center western North Pacific best track data. http://www.usno.navy.mil/NOOC/nmfc-ph/RSS/jtwc/best_tracks/wpindex.php

Kamahori H, Yamazaki N, Mannoji N, Takahashi K (2006) Variability in intense tropical cyclone days in the western North Pacific. SOLA 2:104–107

Kanamitsu M, Ebisuzaki W, Woollen J, Yang S-K, Hnilo JJ, Fiorino M, Potter GL (2002) NCEP-DOE AMIP-II reanalysis (R-2). Bull Am Meteorol Soc 83:1631–1643

Kaplan J, DeMaria M (2003) Large-scale characteristics of rapidly intensifying tropical cyclones in the north Atlantic basin. Weather Forecast 18:1093–1108

Kaplan J, DeMaria M, Knaff JA (2010) A revised tropical cyclone rapid intensification index for the Atlantic and East Pacific basins. Weather Forecast 25:220–241

Klotzbach PJ (2006) Trends in global tropical cyclone activity over the past twenty years (1986–2005). Geophys Res Lett 33:L10805. doi:10.1029/2006GL025881

Klotzbach PJ, Landsea CW (2015) Extremely intense hurricanes: revisiting Webster et al. (2005) after 10 years. J Clim 28:7621–7629. doi:10.1175/JCLI-D-15-0188.1

Knapp KR, Kossin JP (2007) New global tropical cyclone data from ISCCP B1 geostationary satellite observations. J Appl Remote Sens 1:13505–13510

Knapp KR, Kruk MC (2010) Quantifying interagency differences in tropical cyclone best-track wind speed estimations. Mon Weather Rev 138:1459–1473

Kossin JP, Knapp KR, Vimont DJ, Murnane RJ, Harper BA (2007) A globally consistent reanalysis of hurricane variability and trends. Geophys Res Lett 34:L04815. doi:10.1029/2006GL028836

Kossin JP, Olander TL, Knapp KR (2013) Trend analysis with a new global record of tropical cyclone intensity. J Clim 26:9960–9976. doi:10.1175/JCLI-D-13-00262.1

Kossin JP, Emanuel KA, Vecchi GA (2014) The poleward migration of the location of tropical cyclone maximum intensity. Nature 509:349–352

Lander MA (1996) Specific tropical cyclone track types and unusual tropical cyclone motions associated with a reverse-oriented monsoon trough in the western North Pacific. Weather Forecast 11:170–186

Landsea CW (2005) Hurricanes and global warming. Nature 438:E11–E12. doi:10.1038/nature04477

Landsea CW, Harper BA, Hoarau K, Knaff JA (2006) Can we detect trends in extreme tropical cyclones? Science 313:452–454

Lin I-I, Wu C-C, Emanuel KA, Lee I-H, Wu C-R, Pun I-F (2005) The interaction of Supertyphoon Maemi (2003) with a warm ocean eddy. Mon Weather Rev 133:2635–2649. doi:10.1175/MWR3005.1

Lin I-I, Wu C-C, Pun I-F, Ko D-S (2008) Upper-ocean thermal structure and the western North Pacific category 5 typhoons. Part I: ocean features and the category 5 typhoons' intensification. Mon Weather Rev 136:3288–3306. doi:10.1175/2008MWR2277.1

Lin I-I, Black P, Price JF, Yang C-Y, Chen SS, Lien C-C, Harr P, Chi N-H, Wu C-C, D'Asaro EA (2013) An ocean cooling potential intensity index for tropical cyclones. Geophys Res Lett 40:1878–1882. doi:10.1002/grl.50091

Lin I-I, Pun I-F, Lien C-C (2014) "Category-6" supertyphoon Haiyan in global warming hiatus: contribution from subsurface ocean warming. Geophys Res Lett. doi:10.1002/2014GL061281

Lin Y, Zhao M, Zhang M (2015) Tropical cyclone rainfall area controlled by relative sea surface temperature. Nat Commun 6:6591. doi:10.1038/ncomms7591

Liu KS, Chan JCL (2013) Inactive period of western North Pacific tropical cyclone activity in 1998–2011. J Clim 26:2614–2630

McPhaden MJ, Lee T, McClurg D (2011) El Niño and its relationship to changing background conditions in the tropical Pacific Ocean. Geophys Res Lett 38:L15709. doi:10.1029/2011GL048275

Murakami H, Wang B (2010) Future change of North Atlantic tropical cyclone tracks: projection by a 20-km-mesh global atmospheric model. J Clim 23:2699–2721. doi:10.1175/2010JCLI3338.1

Peduzzi P, Chatenoux B, Dao H, De Bono A, Herold C, Kossin J, Mouton F, Nordbeck O (2012) Global trends in tropical cyclone risk. Nat Clim Chang 2:289–294. doi:10.1038/nclimate1410

Price JF (1981) Upper ocean response to a hurricane. J Phys Oceanogr 11:153–175

Price JF, Sanford TB, Forristall GZ (1994) Forced stage response to a moving hurricane. J Phys Oceanogr 24:233–260

Ramage CS (1974) Monsoonal influences on the annual variation of tropical cyclone development over the Indian and Pacific Oceans. Mon Weather Rev 102:745–753

Reynolds RW, Smith TM, Liu C, Chelton DB, Casey KS, Schlax MG (2007) Daily high-resolution-blended analyses for sea surface temperature. J Clim 20:5473–5496

Rienecker MM, Suarez MJ, Gelaro R et al (2011) MERRA: NASA's modern-era retrospective analysis for research and applications. J Clim 24:3624–3648. doi:10.1175/JCLI-D-11-00015.1

Ritchie EA, Holland GJ (1999) Large-scale patterns associated with tropical cyclogenesis in the western Pacific. Mon Weather Rev 127:2027–2043

Rodionov SN (2004) A sequential algorithm for testing climate regime shifts. Geophys Res Lett 31:L09204. doi:10.1029/2004GL019448

RSMC (2015) Regional Specialized Meteorological Centers–Tokyo Typhoon Center western North Pacific best track data. http://www.jma.go.jp/jma/jma-eng/jma-center/rsmc-hp-pub-eg/trackarchives.html

Saji HN, Goswami BN, Vinayachandran PN, Yamagata T (1999) A dipole mode in the tropical Indian Ocean. Nature 401:360–363

Song JJ, Wang Y, Wu L (2010) Trend discrepancies among three best track data sets of western North Pacific tropical cyclones. J Geophys Res 115:D12128. doi:10.1029/2009JD013058

Song JJ, Han JJ, Li SJ, Wang Y, Wu L (2011) Re-examination of trends related to tropical cyclone activity over the western North Pacific basin. Adv Atmos Sci 28:699–708. doi:10.1007/s00376-010-0024-1

Tu JY, Chou C, Huang P, Huang R (2011) An abrupt increase of intense typhoons over the western North Pacific in early summer. Environ Res Lett 6:034013. doi:10.1088/1748-9326/6/3/034013

Wang B, Lin H (2002) Rainy season of the Asian-Pacific summer monsoon. J Clim 15:386–398

Wang B, Zhou X (2008) Climate variability and predictability of rapid intensification in tropical cyclones in the western North Pacific. Meteorol Atmos Phys 99:1–16

Wang B, Kang I-S, Lee J-Y (2004) Ensemble simulations of Asian-Australian monsoon variability by 11 AGCMs. J Clim 17:803–818

Webster PJ, Holland GJ, Curry JA, Chang H-R (2005) Changes in tropical cyclone number, duration and intensity in a warming environment. Science 309:1844–1846

Wu L, Wang B (2008) What has changed the proportion of intense hurricanes in the last 30 years. J Clim 21:1432–1438

Wu L, Zhao H (2012) Dynamically derived tropical cyclone intensity changes over the western North Pacific. J Clim 25:89–98. doi:10.1175/2011JCLI4139.1

Wu M-C, Yeung K-H, Chang W-L (2006) Trends in western North Pacific tropical cyclone intensity. EOS Trans Am Geophys Union 87:537–538. doi:10.1029/2006EO480001

Wu L, Su H, Fovell RG, Wang B, Shen JT, Kahn BH, Hristova-Veleva SM, Lambrigtsen BH, Fetzer EJ, Jiang JH (2012) Relationship of environmental relative humidity with North Atlantic tropical cyclone intensity and intensification rate. Geophys Res Lett 39:L20809. doi:10.1029/2012GL053546

Xu S, Wang B (2014) Enhanced western North Pacific tropical cyclone activity in May in recent years. Clim Dyn 42:2555–2563

Yu L, Jin X, Weller RA (2008) Multidecade global flux datasets from the objectively analyzed air–sea fluxes (OAFlux) project: latent and sensible heat fluxes, ocean evaporation, and related surface meteorological variables. Woods Hole Oceanographic Institution, OAFlux Project Technical Report, OA-2008-01, Woods Hole, MA, 64 p

Zhang Q, Liu Q, Wu L (2009) Tropical cyclone damages in China 1983–2006. Bull Am Meteorol Soc 90:489–495. doi:10.1175/2008BAMS2631.1

Zhao H, Wu L (2014) Inter-decadal shift of the prevailing tropical cyclone tracks over the western North Pacific and its mechanism study. Meteorol Atmos Phys 125:89–101

Zhao H, Wu L, Wang R (2014) Decadal variations of intense tropical cyclones over the Western North Pacific during 1948–2010. Adv Atmos Sci 31:57–65. doi:10.1007/s00376-013-3011-5

Zong H, Wu L (2015) Re-examination of tropical cyclone formation in monsoon troughs over the western North Pacific. Adv Atmos Sci 32:924–934